J Shoulder Elbow Surg (2024) 33, 2493–2504

ELSEVIER

Journal of Shoulder and Elbow Surgery

www.elsevier.com/locate/ymse

A scapular statistical shape model can reliably predict premorbid glenoid morphology in conditions of severe glenoid bone loss

Cole T. Fleet, MESc[a], Théo Giraudon, MSc[b], Gilles Walch, MD[c], Yannick Morvan, PhD[b], Manuel Urvoy, PhD[b], Arnaud Walch, MD[d], Jean-David Werthel, MD, PhD[e], George S. Athwal, MD, FRCSC[f,g,*]

[a]*Department of Mechanical and Materials Engineering, Western University, London, Canada*
[b]*Imascap SAS, Plouzané, France*
[c]*Ramsay Générale de Santé, Jean Mermoz Private Hospital, Centre Orthopédique Santy, Lyon, France*
[d]*Orthopedic Department, Hôpital Edouard Herriot, Lyon, France*
[e]*Orthopedic Department, Hôpital Ambroise Pare, Boulogne-Billancourt, France*
[f]*Roth | McFarlane Hand and Upper Limb Centre, St Joseph's Health Care, London, Canada*
[g]*Department of Surgery, Western University, London, Canada*

Background: Knowledge of premorbid glenoid parameters at the time of shoulder arthroplasty, such as inclination, version, joint line position, height, and width, can assist with implant selection, implant positioning, metal augment sizing, and/or bone graft dimensions. The objective of this study was to validate a scapular statistical shape model (SSM) in predicting patient-specific glenoid morphology in scapulae with clinically relevant glenoid erosion patterns.

Methods: Computed tomography scans of 30 healthy scapulae were obtained and used as the control group. Each scapula was then virtually eroded to create 7 erosion patterns (Walch A1, A2, B2, B3, D, Favard E2, and E3). This resulted in 210 uniquely eroded glenoid models, forming the eroded glenoid group. A scapular SSM, created from a different database of 85 healthy scapulae, was then applied to each eroded scapula to predict the premorbid glenoid morphology. The premorbid glenoid inclination, version, height, width, radius of best-fit sphere, and glenoid joint line position were automatically calculated for each of the 210 eroded glenoids. The mean values for all outcome variables were compared across all erosion types between the healthy, eroded, and SSM-predicted groups using a 2-way repeated measures analysis of variance.

Results: The SSM was able to predict the mean premorbid glenoid parameters of the eroded glenoids with a mean absolute difference of $3° \pm 2°$ for inclination, $3° \pm 2°$ for version, 2 ± 1 mm for glenoid height, 2 ± 1 mm for glenoid width, 5 ± 4 mm for radius of best-fit sphere, and 1 ± 1 mm for glenoid joint line. The mean SSM-predicted values for inclination, version, height, width, and radius were not significantly different than the control group ($P > .05$).

Discussion: An SSM has been developed that can reliably predict premorbid glenoid morphology and glenoid indices in patients with common glenoid erosion patterns. This technology can serve as a useful template to visually represent the premorbid healthy glenoid in

Institutional review board approval was not required for this computer modeling study.

*Reprint requests: George S. Athwal, MD, FRCSC, Roth | McFarlane Hand and Upper Limb Centre, St Joseph's Health Care, 268 Grosvenor St, London, ON N6A 4V2, Canada.
E-mail address: gsathwal@hotmail.com (G.S. Athwal).

https://doi.org/10.1016/j.jse.2024.03.060

patients with severe glenoid bony erosions. Knowledge of the premorbid glenoid preoperatively can assist with implant selection, positioning, and sizing.

Level of evidence: Anatomy Study; Computer Modeling

Keywords: Statistical shape model; glenoid erosion; glenoid morphology; shoulder arthroplasty; preoperative planning; rotator cuff tear arthropathy; osteoarthritis

Glenoid erosions are commonly observed with glenohumeral osteoarthritis (GHOA) and cuff tear arthropathy (CTA). Classifications, such as the Walch[4] and Favard[44] systems, have been created to categorize different glenoid erosion patterns associated with GHOA and CTA, respectively. Patients with these pathologies often suffer from pain and reduced shoulder function. Total shoulder arthroplasty (TSA) and reverse shoulder arthroplasty (RSA) can be used for the treatment of such pathologies. It has been reported that glenoid component positioning is important for success, as implant malposition has been identified as a factor leading to inferior outcomes.[5,19,52]

In TSA, optimized placement of the glenoid component is important to minimize eccentric joint loading that can lead to component loosening and instability due to the rocking-horse mechanism.[9,16,19,33,41] Therefore, knowledge of the premorbid glenoid can potentially aid in surgical decision making and preoperative planning of glenoid component placement. Anatomic restoration of the joint line in TSA is also important for restoring adequate rotator cuff and deltoid tension, and thus joint reaction forces.[15] In RSA, superior inclination of the glenoid baseplate has been shown to increase implant-bone interface stresses[13,22] and increase the risk for scapular notching and subsequent component loosening.[28] The optimized location of the RSA implant in relation to the premorbid joint line in the eroded glenoid is presently not well understood; however, it is known that muscles crossing the joint may function more efficiently when their anatomy is restored. Knowledge of the premorbid joint line position, therefore, can assist in implant selection and position to restore soft tissue relationships. In the future, knowledge of the premorbid glenoid, the intraoperative position of the implants, and the eventual postoperative outcome will allow artificial intelligence algorithms to predict the patient-specific ideal position of implants to provide the best possible outcomes.

Presently, it can be very difficult in patients with severe glenoid bone loss to predict premorbid glenoid morphology.[17] Previous groups have shown that the contralateral shoulder can be used to predict premorbid glenoid morphology,[51] although this approach is limited to patients with a healthy contralateral scapula with available bilateral shoulder computed tomography (CT) scans. In 2008, Codsi et al[7] developed a glenoid vault model to characterize the healthy shape of the glenoid vault. This model has since been validated for quantifying premorbid glenoid inclination, version, joint line medialization, and glenoid bone loss in arthritic glenoids,[10,18,37,39,40] although the model needs to be manually aligned with the pathologic glenoid. Perhaps the most common tool in recent years used to predict premorbid glenoid morphology is a statistical shape model (SSM). These models capture the average shape and the common shape variances of a specific object across a sample population. Recently, several groups[2,35,38,48] have used scapular SSMs for predicting premorbid glenoid morphology in patients with glenoid bone loss. However, these studies did not evaluate their models using Walch or Favard erosions patterns in which the patient-specific premorbid glenoid morphology was known. Therefore, the purpose of this study was to validate the accuracy of a scapular SSM in predicting premorbid glenoid morphology in scapulae with various Walch- or Favard-type glenoid erosion patterns. The SSM validation procedure used in this study served to allow for the direct comparison between the premorbid and SSM-predicted glenoid morphology.

Materials and methods

Healthy scapulae group

CT scans of 30 healthy scapulae were obtained to comprise the control glenoid group. These healthy scapulae were used to create all virtual glenoid erosions in proceeding steps. Furthermore, these scapulae represented the true premorbid glenoid morphology and were used to assess the accuracy of the scapular SSM to predict premorbid morphology in this study. The average age of this group was 41 $\pm$ 16 years, and was evenly split between male and female, and right and left scapulae. The mean, standard deviation, and range of various glenoid parameters from this control group are provided in Table I. Exclusion criteria for this study included GHOA, CTA, glenohumeral instability, scapula fractures, and humeral head pathology. CT scans exhibiting truncated scapulae were also excluded to ensure consistency across the control group. All scans were obtained using the following parameters: slice thickness $<$1.2 mm, number of slices $>$200, X-Y resolution $<$0.5 mm, matrix size: 512 $\times$ 512, tube peak voltage = 140 kV, and tube current $>$300 mA. All scans were uploaded into a validated surgical preoperative planning software (Glenosys, v.10.6.1; Imascap, Plouzané, France), where all scans were automatically segmented to obtain 3-dimensional (3D) models of each healthy scapula and humerus.

Table I Mean parameters for the control scapula group

Parameter	Mean	SD	Range (min, max)
Age, yr	41	16	19, 85
Inclination, degrees	10	5	−3, 19
Version, degrees	−6	4	−1, −15
Glenoid radius of best-fit sphere, mm	33	5	26, 45
Glenoid height, mm	35	4	28, 43
Glenoid width, mm	27	3	20, 37

SD, standard deviation.

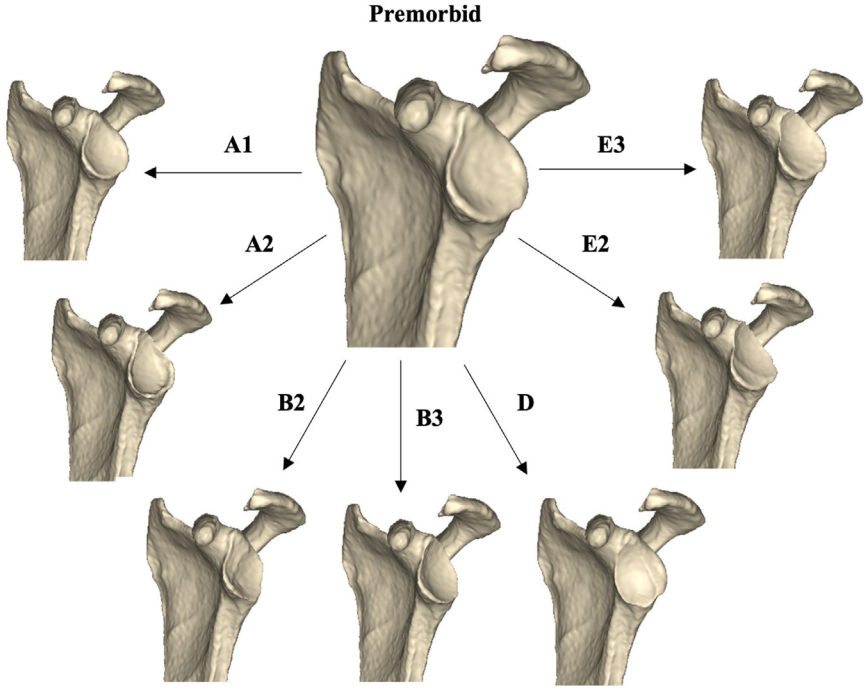

Figure 1 Each scapula in the premorbid cohort was virtually eroded to create 7 unique glenoid erosion patterns, resulting in 7 pathologic scapulae for each premorbid scapula model. Erosion patterns correspond to those described by the Walch and Favard classifications.

Virtual glenoid erosions

To obtain the eroded group for this study, the glenoid of each healthy scapula was virtually eroded 7 different times to create 7 unique glenoid erosion patterns according to the Walch and Favard classifications for GHOA and CTA, respectively. The specific erosion patterns created in this study included type A1, A2, B2, B3, D, E2, and E3 erosions (Fig. 1). This allowed for 30 unique glenoid erosions for each erosion pattern to be created from each healthy scapula, resulting in a total of 210 eroded glenoids (eroded glenoid group). To create each erosion, the healthy proximal humerus for each corresponding healthy scapula was rotated to approximately 45° of glenohumeral abduction as this was observed to maximize the contact between articular surfaces on both sides of the joint (Fig. 2). The plane of abduction, in addition to the medialization, anterior-posterior, and superior-inferior translation of the proximal humerus were adjusted depending on the specific type of erosion being created. Once the overlapping volume of the proximal humerus relative to the glenoid was deemed adequate, a Boolean subtraction was performed between the 2 objects. This resulted in an elliptical erosion pattern to be created on the face of the glenoid. All virtual erosions were visually evaluated by the senior author prior to use in this study.

In addition to the different erosion patterns generated, all virtual erosions were created to satisfy specifications for each erosion pattern. The erosion specifications used in this study are described in Table II. These specifications were created to capture the variations in these specific erosion patterns previously observed in literature[1,4,25,32] and to vary the severity of bone loss for each case. The medialization of the proximal humerus, or erosion depth, was specified for all erosion types. Erosion depths were specified between 4 and 8 mm for all types excluding type A1 erosions. Erosion depths for this group were specified between 1 and 3 mm as these erosions are less severe.[4] Additional erosion parameters were specified for type B2, D, and E2 patterns (Fig. 3). B2 erosions were additionally characterized by the size of the neoglenoid surface relative to that of the entire glenoid surface, as

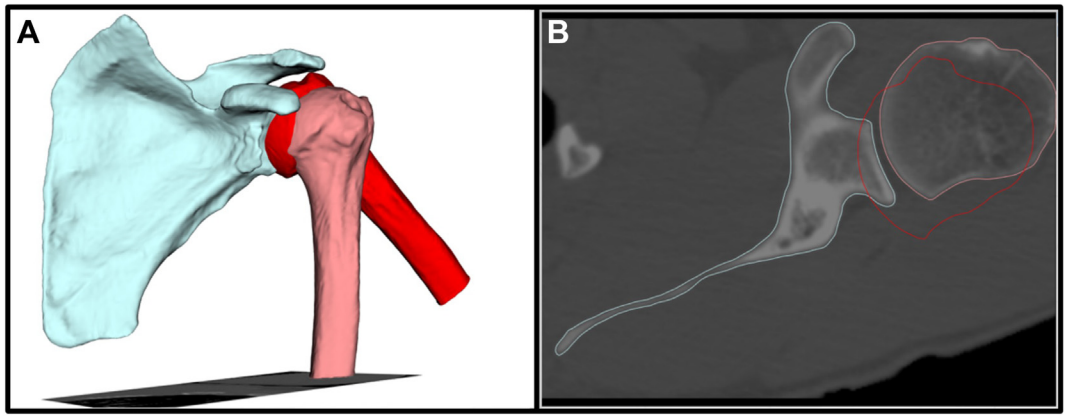

Figure 2 (**A**) A 3D rendering of the premorbid healthy scapula and humerus during creation of a virtual erosion. The humerus was rotated to 45° of glenohumeral abduction from its initial position and translated medially to overlap with part of the glenoid. (**B**) The resulting overlap is illustrated on an axial computed tomography image with the (*red outline*) of the humeral head.

Table II Specific characteristics for each erosion pattern evaluated

Erosion pattern	Medialization, mm	Neoglenoid size	Concavity type	Neoglenoid location
A1	1, 2, and 3			
A2	4, 6, and 8			
B2	4, 5, and 6	Mild, moderate, and severe		
B3	4, 6, and 8			
D	4, 6, and 8		Monoconcave and biconcave	
E2	4, 5, and 6			Superior, anterosuperior, and posterosuperior
E3	4, 6, and 8			

previously described by Knowles et al.[25] The translation of the proximal humerus in the anterior-posterior and superior-inferior directions was adjusted for this parameter. Type D erosion patterns were created as either monoconcave or biconcave, as both types have previously been reported.[32] The location of the neoglenoid relative to the paleoglenoid in E2-type erosions was also varied. The neoglenoid was created either directly superiorly to the paleoglenoid or with an anterosuperior or posterosuperior offset.[1] All specifications were randomly assigned to the healthy scapula models before creating the virtual erosions.

Scapular SSM generation and application

The SSM used in this study was created using a database of 85 healthy scapula CT scans of which 59 were right scapulae and 26 were left scapulae. None of the scapulae used to create this model were used in the control group of this study. All scans were manually segmented (Amira, v. 5.3.3; VSG–Visualization Sciences Group, Burlington, MA, USA) and 3D models of each scapula were created. From here, the mean scapula shape was determined with 23 modes that captured the variation in scapular shape variance among the population.

The scapular SSM was then used to predict the premorbid shape of each scapula in the eroded group. To accomplish this, the SSM was automatically fitted to each eroded scapula within the preoperative planning software. This process consists of a nonlinear optimization algorithm that adjusts the position, rotation, and modes of variance of the SSM in order to achieve an optimized alignment between the medial scapular bodies of the SSM and target scapula. The medial scapula body was used in this alignment algorithm as these regions of the scapula are less susceptible to changes in osseous morphology due to GHOA and CTA. Once this process was complete, the scapular SSM was displayed on both a 3D model and 2D CT views of each scapula from the eroded group (Fig. 4). The glenoid from the SSM then served as a premorbid prediction for the eroded scapula.

Outcome variables and statistical analysis

The primary outcome variables for this study included glenoid inclination, version, height, width, radius of best-fit sphere, and the change in joint line position. All variables were automatically computed in the preoperative planning software for all 3 glenoid groups assessed in this study. The glenoid radius of the best-fit

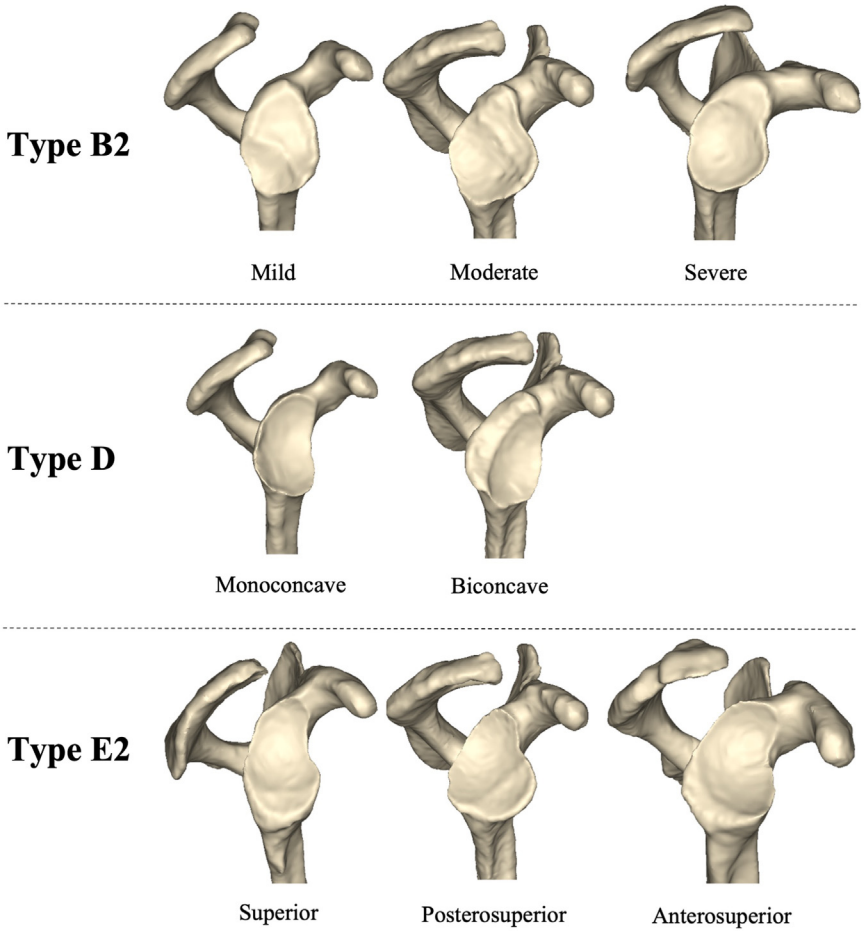

Figure 3 3D models of the clinically relevant erosions used to test the statistical shape model predictions. Pictured are Walch B2, Walch D, and Favard E2 type erosions.

sphere was used to characterize the average curvature of the glenoid articular surface. The size of the best-fit sphere was computed using an algorithm that minimized the sum of squared errors in distance between points on the glenoid articular surface and the sphere of best fit.[29,30] The change in joint line position was expressed relative to the position of the joint line for each control glenoid. This was done to provide a clinically relevant meaning to this variable as opposed to expressing the cartesian coordinates of this location within the CT scanner coordinate system. Therefore, the location of the joint line position for each control glenoid was expressed with a value of 0, which was found not to influence the results of the statistical analysis conducted. To quantify the change in joint line position, a glenoid coordinate system was automatically created in the preoperative planning software for each glenoid in the control group. The change in joint line position was then defined as the translation of the glenoid center, for both pathologic and SSM-predicted glenoid groups, along the medial-lateral axis of the control glenoid's coordinate system. A lateral change in joint line position was expressed as positive while a medial change in joint line position was expressed as negative. The glenoid height and width were calculated as the distance between opposing points on the glenoid rim in the superior-inferior and anterior-posterior directions of the glenoid coordinate system, respectively.

Statistical analysis was performed using SPSS software (IBM, Armonk, NY, USA) in which a 2-way repeated measures analysis of variance was performed. The independent variables were the glenoid group (control group, pathologic group, and SSM-predicted group) and erosion type. A Bonferroni adjustment was performed to account for multiple comparisons with statistical significance set to $P \leq .05$.

Results

Mean results for control, pathologic, and SSM-predicted groups

The mean values for glenoid inclination, version, height, width, radius of best-fit sphere, and joint line position are reported in Table III for all glenoid groups and erosion patterns.

As expected, statistically significant differences were identified between the healthy control and the eroded glenoid groups (Table III). The mean inclination values between control and eroded glenoid groups were statistically significant for all erosion patterns ($P \leq .001$) except for

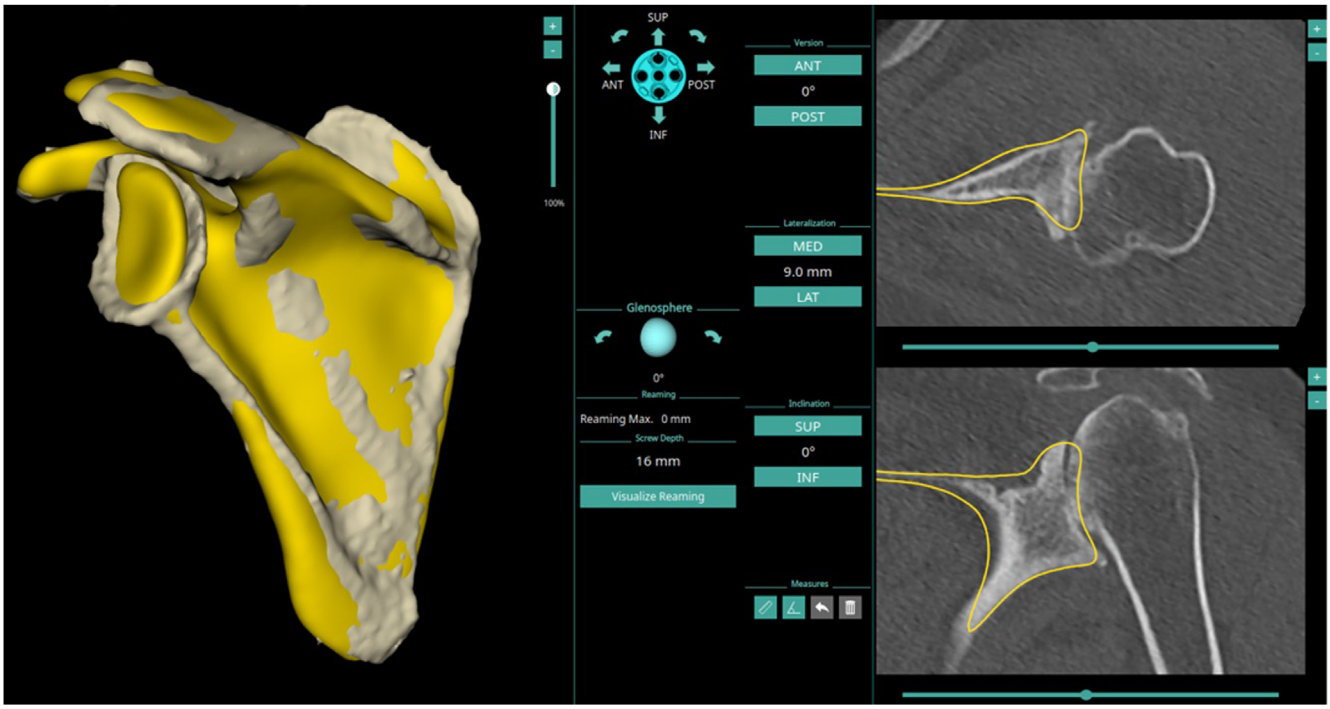

Figure 4 Illustration of the scapular statistical shape model (*yellow*) projected onto the target scapula within a preoperative planning software program. The left image displays the 3D projection of the scapular statistical shape model onto the target scapula body, whereas the 2D images show the border of the scapular statistical shape model prediction onto the axial (top right) and coronal (bottom right) computed tomography scans of the target scapula.

Table III Mean outcome values for healthy control, eroded, and SSM-predicted glenoid cohorts

	Inclination, degrees	Version, degrees	Glenoid radius of best-fit sphere, mm	Glenoid height, mm	Glenoid width, mm	Joint line position, mm
Healthy (n = 30)	10 ± 5	−6 ± 4	33 ± 5	35 ± 4	27 ± 3	
Eroded (n = 210)						
A1	10 ± 5	−7 ± 4	28 ± 3*	36 ± 3	28 ± 3	−1 ± 1*
A2	9 ± 6	−4 ± 5*	25 ± 3*	38 ± 4*	27 ± 3	−5 ± 2*
B2	6 ± 6*	−14 ± 6*	27 ± 6*	38 ± 4*	27 ± 3	−2 ± 2*
B3	14 ± 7*	−21 ± 6*	25 ± 2*	37 ± 3*	27 ± 3	−5 ± 2*
D	3 ± 7*	9 ± 6*	24 ± 4*	38 ± 4*	28 ± 4	−2 ± 3*
E2	22 ± 6*	−8 ± 8	28 ± 4*	38 ± 4*	29 ± 3*	−3 ± 1*
E3	20 ± 5*	−4 ± 4*	28 ± 6*	37 ± 4*	29 ± 4*	−4 ± 2*
SSM (n = 210)						
A1	10 ± 5	−6 ± 3	32 ± 7	35 ± 3	27 ± 3	0 ± 1
A2	10 ± 4	−7 ± 3	32 ± 8	35 ± 4	27 ± 3	−1 ± 1*
B2	10 ± 4	−7 ± 3	31 ± 7	35 ± 3	27 ± 3	−1 ± 1*
B3	10 ± 5	−6 ± 3	31 ± 8	35 ± 3	27 ± 2	−1 ± 1*
D	10 ± 4	−7 ± 3	30 ± 8*	35 ± 3	27 ± 3	−1 ± 1*
E2	11 ± 4	−6 ± 3	32 ± 8	35 ± 3	27 ± 3	−1 ± 1*
E3	11 ± 4	−6 ± 4	32 ± 8	35 ± 3	27 ± 3	−1 ± 1*

SSM, statistical shape model.
* $P \leq .05$ relative to the corresponding premorbid value.

type A1 and A2 erosions ($P > .99$). This was similar for version, as all erosion types, excluding type A1 and E2 ($P > .99$), had significantly different version compared with the control glenoid group ($P \leq .036$). Statistically significant differences were detected between the control group and all erosion patterns for the mean values of the

radius of the best-fit glenoid sphere ($P \leq .001$) and joint line position ($P \leq .002$). All erosion patterns, except for type A1 ($P = .277$), exhibited significantly different glenoid height as compared to the control glenoid group ($P \leq .001$).

In 4 of 6 glenoid metrics, the SSM prediction of the premorbid glenoid was not significantly different from that of the healthy control group (Table III). No statistically significant differences for any erosion type were observed between the control and the SSM prediction for the mean values of glenoid inclination ($P \geq .721$), version ($P > .99$), height ($P > .99$), and width ($P \geq .078$). The average radius of the best-fit sphere for the SSM prediction with type D erosions, however, was significantly different from that of the control group ($P = .030$). For all other erosions, there were no significant differences ($P \geq .171$) with the SSM prediction. The glenoid joint line position was predicted using the scapular SSM to within -1 ± 1 mm of the control group for all erosion patterns. However, the SSM prediction of the joint line position for all erosion patterns was significantly different compared with the control group ($P \leq .010$), except for the type A1 erosion pattern ($P > .99$).

Mean absolute differences relative to the control glenoid group

The mean absolute differences for both the pathologic and SSM-predicted glenoid cohorts relative to the control cohort for all outcome variables and erosion patterns are presented in Fig. 5. For the pathologic group, the mean absolute difference relative to the control group for glenoid inclination, version, height, width, radius of best-fit sphere, and joint line were $7^\circ \pm 5^\circ$, $7^\circ \pm 7^\circ$, 2 ± 2 mm, 2 ± 2 mm, 7 ± 4 mm, and 3 ± 2 mm, respectively. When the scapular SSM was applied, these mean absolute differences were significantly reduced for inclination ($3^\circ \pm 2^\circ$, $P < .001$), version ($3^\circ \pm 2^\circ$, $P < .001$), glenoid radius of best-fit sphere ($5^\circ \pm 4^\circ$, $P = .018$), joint line position ($1^\circ \pm 1^\circ$, $P < .001$), and glenoid height ($1^\circ \pm 1^\circ$, $P < .001$) but not for glenoid width ($2^\circ \pm 1^\circ$, $P = .883$).

The type of glenoid erosion was not found to significantly influence the prediction of the premorbid glenoid using the scapular SSM for glenoid inclination ($P > .99$), version ($P > .99$), best-fit sphere radius ($P > .99$), height ($P > .99$), or width ($P > .99$). However, statistically significant differences in the mean absolute joint line position error were observed between type A1 erosions (1 ± 1 mm) and type A2 (1 ± 1 mm, $P = .005$) and E3 (1 ± 1 mm, $P = .014$) erosions.

Discussion

Scapular SSMs are a useful tool for determining the average shape and common shape variations across a sample population. They can also be used for several other purposes, including the quantification of glenoid bone loss,[36] predicting scapular bone density distribution,[42,45] and to correlate premorbid glenoid anatomy to humeral head translation[49,50] and erosion patterns.[47] However, the ability of an SSM to be overlapped with the normal regions of a patient's bone, which then highlights the differences between the SSM-predicted premorbid anatomy and the pathologic bone, may be one of the most important functions of this model.

This study validated the accuracy of a scapular SSM in predicting premorbid glenoid morphology in patients with GHOA or CTA. The methods used provide a strong validation of this model. The SSM was evaluated against 7 different erosion patterns observed clinically. Furthermore, 30 unique erosions were created for each erosion type, all of which captured various morphologic attributes that have previously been clinically observed. This further increased the variability of glenoid erosion patterns against which the SSM was validated. Additionally, the creation of these erosions from healthy scapulae allowed the prediction of the SSM to be compared directly to the known premorbid ground truth glenoid as opposed to average healthy glenoid parameters. This fully automated SSM can eventually be integrated into preoperative planning software and can thus be used as a patient-specific template for premorbid glenoid morphology, which can assist with preoperative planning in TSA and RSA.

SSMs have previously been investigated for predicting glenoid bone loss. Abler et al[2] used a scapular SSM to predict premorbid glenoid morphology in scapulae with glenoid erosion patterns described by the Walch classification. However, the SSM was only validated using 30 glenoid erosions, which limits the robustness of the validation. This prevented the authors from forming any conclusions regarding specific erosion patterns. Furthermore, clinical erosions models were used that prevented the SSM prediction from being compared directly to the known premorbid ground true glenoid morphology. Instead, glenoid metrics from a separate cohort of healthy scapulae were used to approximate premorbid glenoid parameters. Our study used 30 unique erosions for each of the 7 erosion types investigated, allowing the SSM to be evaluated against a total of 210 different eroded glenoids. Furthermore, these erosions were virtually created from healthy scapulae, allowing the SSM prediction to be compared to the known premorbid ground truth glenoid morphology in each case.

Plessers et al[35] also evaluated an SSM in predicting premorbid glenoid morphology in scapulae with Wallace-type bone defects.[26] In their study, all defects were virtually created on healthy scapulae, allowing the scapular SSM prediction to be compared directly to the premorbid scapular anatomy, similar to the methods used in our study. However, the healthy scapula cohort used to construct the SSM was also used to evaluate the model, which required a leave-one-out approach to be used for

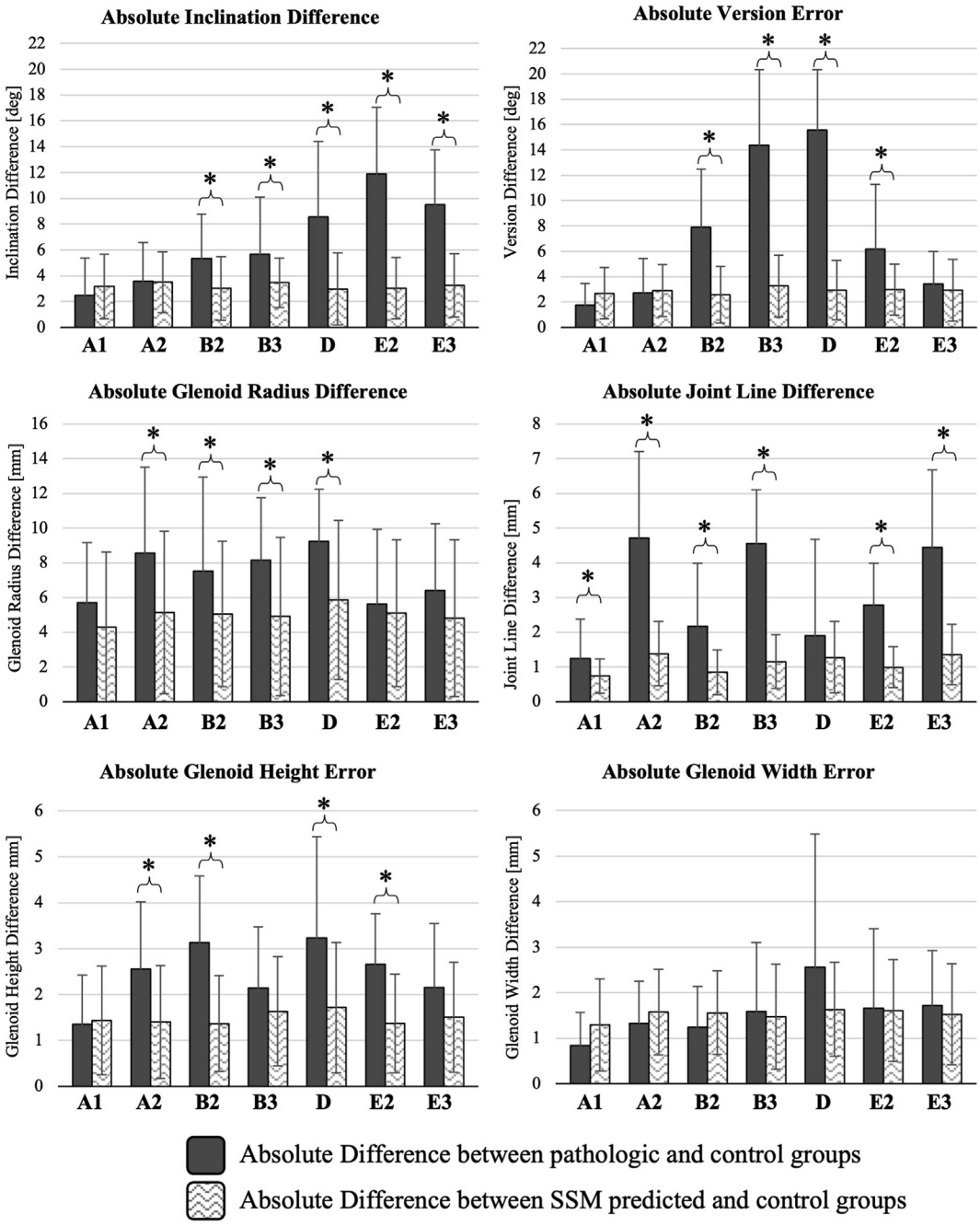

Figure 5 These plots illustrate the mean (±1 standard deviation) absolute difference for both the pathologic and statistical shape model (SSM)-predicted cohorts relative to the control group for all outcome variables (moving clockwise from the top left corner: glenoid version, glenoid inclination, glenoid medialization, glenoid width, glenoid height, glenoid radius of BFS). *Statistically significant difference ($P \leq .05$).

comparisons between healthy and SSM predictions. We used a unique cohort of healthy scapula for the SSM development, and then used a different test cohort for experimental evaluation. This was done to avoid any potential bias in the comparative results, and to ensure the SSM would be effective with any glenoid, not only in the glenoids used to create the model.

Prior to SSMs, other methods to predict premorbid glenoid morphology in patients with glenoid bone loss were investigated. Use of the contralateral scapula as a template for premorbid glenoid anatomy in patients with unilateral scapula pathology has previously been investigated. Verhaegen et al[51] reported mean differences of 2° for both inclination and version, and 2 mm of scapular

offset between healthy bilateral scapulae. These results support the use of the contralateral scapula to be used as a patient-specific template for predicting premorbid glenoid morphology. Several other studies have also reported findings suggesting contralateral scapulae share similar glenoid morphologic parameters, especially when pertaining to parameters related to glenohumeral instability.[27,34,43] However, use of the contralateral scapula can only be used in patients with a normal contralateral shoulder, which oftentimes is not present. Furthermore, the use of the contralateral scapula as a template for premorbid glenoid morphology requires bilateral CT scans to be obtained and requires software to create a reciprocal model.

Another alternative to a scapular SSM includes the glenoid vault model developed by Codsi et al.[7] In this study, Codsi and colleagues found the glenoid vault to exhibit a consistent, and when scaled, congruent shape between healthy patients. From this, the authors developed a 3D template of the glenoid vault that could be scaled and virtually implanted into patient scapulae. This model has since been used to predict several premorbid glenoid parameters and quantify glenoid bone loss in patients with GHOA. Scalise et al[39,40] reported the glenoid vault model to predict glenoid bone loss and premorbid glenoid version with errors of 1% and 2°, respectively, while using the nonarthritic contralateral scapula as a template for normal glenoid vault anatomy. Additional studies have also used this model to predict premorbid glenoid version, inclination, and joint line medialization in patients with GHOA.[10,18,37] This model, however, has not yet been validated in patients with CTA and requires manual positioning on the CT scan. Gilliland et al[12] also proposed a technique for predicting premorbid joint line. They identified a set of healthy scapular landmarks that can potentially be used to predict glenoid joint line in patients with significant joint line medialization due to glenoid erosion. However, this method has not yet been validated on pathologic scapulae.

Although all variables assessed in this study are important in quantifying total premorbid glenoid morphology, knowledge of premorbid glenoid inclination, version, and joint line are perhaps the most important for deciding implant selection and position in shoulder arthroplasty. In TSA, failure to adequately correct glenoid retroversion, especially in cases of severe posterior glenoid wear, can result in eccentric joint loading, leading to subsequent component loosening and glenohumeral instability.[9,16,19,33,41] Although it is debated as to whether version should be corrected to premorbid values within these patients,[24,37] knowledge of the premorbid glenoid can aid in surgical planning and decision making. Glenoid joint line re-creation can be especially difficult in severe B3 erosions, which can exhibit significant glenoid retroversion.[6] Additionally, malposition of the glenoid component in inclination has also been shown to lead to increased eccentric joint forces and muscle loading.[20,23] Knowledge of the premorbid joint line is also valuable in both TSA and RSA. In TSA, medialization of the joint line can lead to rotator cuff muscular shortening, increased rotator cuff and deltoid loading, and increased eccentric joint loading due to a change in deltoid line of action.[15] In contrast, overlateralization may overtension the rotator cuff, leading to increased joint loading and cuff failure. Excessive medialization in RSA decreases rotator cuff tension and glenohumeral stability,[3] while also increasing the risk for scapular notching.[28] Lateralization of the joint line in RSA reduces the risk for scapular notching but can potentially increase the risk for scapular spine fracture[21,53,54] and increase shear loading on the glenoid baseplate.[14] Although the goal in RSA is not to restore the joint line to its premorbid state, understanding of its location can help to improve implant selection and placement. Additionally, understanding premorbid anatomy, the postoperative position of implants, and the final patient outcomes can assist in artificial intelligence algorithms to customize implant location to optimize postoperative outcome parameters.

In our study, we demonstrated that a scapular SSM can be effective in predicting premorbid inclination, version, and joint line position for the virtual glenoid erosions created to mimic those commonly encountered in GHOA and CTA. The mean absolute error for the SSM prediction in version and inclination across all erosion types was 3° ± 2° and 3° ± 2°, respectively. Additionally, absolute mean version errors of 3° ± 2° and 3° ± 2° were observed for type B2 and B3 erosions, respectively—patterns for which predicting premorbid glenoid version can be difficult because of significant posterior glenoid wear and retroversion. If the mean values of inclination (10°) and version (–6°) from the healthy glenoid cohort were used to predict premorbid glenoid anatomy, one could experience errors as great as 13° for inclination and 9° for version because of the large variance of these parameters in the healthy glenoid cohort (Table I), which has also previously been reported.[11] The SSM was also highly accurate in its ability to predict the premorbid glenoid joint line, such that the prediction was an absolute mean of 1 ± 1 mm different from the control. This difference was found to be statistically significant ($P \leq .010$); however, we believe that the 1-mm difference in joint line may not be clinically substantial. Overall, understanding of the joint line location is especially important in cases of severe glenoid erosions, such as in A2, B3, and E3 cases, where there is no remaining paleoglenoid for estimation.

The scapular SSM was also accurate in predicting premorbid glenoid morphology in all virtual erosion types evaluated in this study. No statistically significant differences in the mean absolute error relative to the control group were observed between the various erosion types for glenoid inclination, version, radius of best-fit sphere, height, and width. Type A2 and E3 erosions were observed

to exhibit significantly greater absolute error in predicting premorbid joint position (1 ± 1 mm) compared with type A1 erosions (1 ± 1 mm, $P \leq .014$). However, as previously discussed, these differences are likely not clinically relevant.

This study is not without limitations. Perhaps the greatest limitation of this study was the inability to use true glenoid erosion cases for our eroded glenoid group. All erosion patterns were virtually created in this study using a Boolean subtraction between corresponding healthy glenoid and humerus models. This method does not simulate the unconstrained translation and rotation of the humerus, which contributes to glenoid erosion in these patients. Furthermore, patients with glenoid erosion can present with osteophyte formation around the periphery of the glenoid, which may influence the morphology of the glenoid. Although the techniques used in this study may not precisely replicate the true morphology of a pathologic glenoid, we believe they provide a strong initial validation of this scapular SSM across a large group of varying glenoid erosion patterns. Perhaps the next step in validating the accuracy and precision of this scapular SSM will be to apply this model to patients exhibiting unilateral glenoid erosion due to GHOA or CTA, for which the premorbid glenoid morphology can be inferred using a healthy contralateral scapula.[39,40,51] This study was also limited in that bone was only removed from the glenoid for all erosion types evaluated. However, in patients with CTA, erosion of the acromion and possibly coracoid can occur as a result of superior migration of the humeral head.[31] This should have minimal impact on the SSM prediction, however, as the SSM uses the morphology of the medial scapular body to align and predict the SSM to the pathologic scapula. Lastly, the scapular SSM evaluated in this study was only used to predict premorbid glenoid morphology in scapulae exhibiting common glenoid erosion patterns due to GHOA or CTA. This SSM in theory could also be used to predict premorbid glenoid morphology in cases of glenohumeral instability with glenoid bone loss. Further study is needed to validate this SSM's ability to predict clinically relevant morphologic parameters of the glenoid, such as glenoid inferior best-fit circle and diameter,[8,46] in scapulae with anterior and posterior glenoid bone loss.

Conclusion

The results from this study provide an initial validation that predictive statistical shape modeling of the arthritic eroded glenoid can be an effective technique in determining premorbid glenoid parameters, such as inclination, version, and dimensions, with a high degree of precision. Further study is needed to better validate this scapular SSM in predicting premorbid glenoid bone in patient scapulae with glenoid erosions. Once validated clinically, this technology can be used to visualize a 3D patient-specific representation of the premorbid healthy glenoid, which can assist surgeons with implant selection and placement during shoulder arthroplasty.

Acknowledgment

The authors would like to acknowledge the IMASCAP support team for their work and assistance during the creation of all virtual glenoid erosions.

Disclaimers:

Funding: No funding was disclosed by the authors.
Conflicts of interest: Gilles Walch, Jean-David Werthel, and George Athwal are paid consultants and receive royalties for shoulder arthroplasty design from Stryker. Theo Giraudon, Manuel Urvoy, and Yannick Morvan are paid employees for Stryker. The other authors, their immediate families, and any research foundations with which they are affiliated did not receive any financial payments or other benefits from any commercial entity related to the subject of this article.

References

1. Abdic S, Knowles NK, Walch G, Johnson JA, Athwal GS. Type E2 glenoid bone loss orientation and management with augmented implants. J Shoulder Elbow Surg 2020;29:1460-9. https://doi.org/10.1016/j.jse.2019.11.009
2. Abler D, Berger S, Terrier A, Becce F, Farron A, Büchler P. A statistical shape model to predict the premorbid glenoid cavity. J Shoulder Elbow Surg 2018;27:1800-8. https://doi.org/10.1016/j.jse.2018.04.023
3. Bauer S, Corbaz J, Athwal GS, Walch G, Blakeney WG. Lateralization in reverse shoulder arthroplasty. J Clin Med 2021;10:5380. https://doi.org/10.3390/jcm10225380
4. Bercik MJ, Kruse K, Yalizis M, Gauci MO, Chaoui J, Walch G. A modification to the Walch classification of the glenoid in primary glenohumeral osteoarthritis using three-dimensional imaging. J Shoulder Elbow Surg 2016;25:1601-6. https://doi.org/10.1016/j.jse.2016.03.010
5. Boileau P. Complications and revision of reverse total shoulder arthroplasty. Orthop Traumatol Surg Res 2016;102(1 Suppl):S33-43. https://doi.org/10.1016/j.otsr.2015.06.031
6. Chan K, Knowles NK, Chaoui J, Ferreira LM, Walch G, Athwal GS. Is the Walch B3 glenoid significantly worse than the B2? Shoulder Elbow 2018;10:256-61. https://doi.org/10.1177/1758573217724111
7. Codsi MJ, Bennetts C, Gordiev K, Boeck DM, Kwon Y, Brems J, et al. Normal glenoid vault anatomy and validation of a novel glenoid implant shape. J Shoulder Elbow Surg 2008;17:471-8. https://doi.org/10.1016/j.jse.2007.08.010
8. Ernat JJ, Golijanin P, Peebles AM, Eble SK, Midtgaard KS, Provencher MT. Anterior and posterior glenoid bone loss in patients

receiving surgery for glenohumeral instability is not the same: a comparative 3-dimensional imaging analysis. JSES Int 2022;6:581-6. https://doi.org/10.1016/j.jseint.2022.02.007
9. Farron A, Terrier A, Büchler P. Risks of loosening of a prosthetic glenoid implanted in retroversion. J Shoulder Elbow Surg 2006;15:521-6. https://doi.org/10.1016/j.jse.2005.10.003
10. Ganapathi A, McCarron JA, Chen X, Iannotti JP. Predicting normal glenoid version from the pathologic scapula: a comparison of 4 methods in 2- and 3-dimensional models. J Shoulder Elbow Surg 2011;20:234-44. https://doi.org/10.1016/j.jse.2010.05.024
11. Gauci MO, Deransart P, Chaoui J, Urvoy M, Athwal GS, Sanchez-Sotelo J, et al. Three-dimensional geometry of the normal shoulder: a software analysis. J Shoulder Elbow Surg 2020;29:e468-77. https://doi.org/10.1016/j.jse.2020.03.042
12. Gilliland L, Launay M, Salhi A, Green N, Maharaj J, Italia KR, et al. Restoration of glenoid joint line: a three-dimensional analysis of scapular landmarks. JSES Int 2023;7:478-84. https://doi.org/10.1016/j.jseint.2023.01.012
13. Gutiérrez S, Walker M, Willis M, Pupello DR, Frankle MA. Effects of tilt and glenosphere eccentricity on baseplate/bone interface forces in a computational model, validated by a mechanical model, of reverse shoulder arthroplasty. J Shoulder Elbow Surg 2011;20:732-9. https://doi.org/10.1016/j.jse.2010.10.035
14. Harman M, Frankle M, Vasey M, Banks S. Initial glenoid component fixation in "reverse" total shoulder arthroplasty: a biomechanical evaluation. J Shoulder Elbow Surg 2005;14(1S):S162-7. https://doi.org/10.1016/j.jse.2004.09.030
15. Hasler A, Bachmann E, Ker A, Viehöfer AF, Wieser K, Gerber C. Joint-line medialization after anatomical total shoulder replacement requires more rotator cuff activity to preserve joint stability. JSES Int 2021;5:406-12. https://doi.org/10.1016/j.jseint.2020.11.010
16. Ho JC, Sabesan VJ, Iannotti JP. Glenoid component retroversion is associated with osteolysis. J Bone Joint Surg Am 2013;95:e82. https://doi.org/10.2106/JBJS.L.00336
17. Iannotti JP, Greeson C, Downing D, Sabesan V, Bryan JA. Effect of glenoid deformity on glenoid component placement in primary shoulder arthroplasty. J Shoulder Elbow Surg 2012;21:48-55. https://doi.org/10.1016/j.jse.2011.02.011
18. Iannotti JP, Jun BJ, Patterson TE, Ricchetti ET. Quantitative measurement of osseous pathology in advanced glenohumeral osteoarthritis. J Bone Joint Surg Am 2017;99:1460-8. https://doi.org/10.2106/JBJS.16.00869
19. Iannotti JP, Spencer EE, Winter U, Deffenbaugh D, Williams G. Prosthetic positioning in total shoulder arthroplasty. J Shoulder Elbow Surg 2005;14(1 SUPPL):S111-21. https://doi.org/10.1016/j.jse.2004.09.026
20. Karelse A, Van Tongel A, Verstraeten T, Poncet D, De Wilde LF. Rocking-horse phenomenon of the glenoid component: the importance of inclination. J Shoulder Elbow Surg 2015;24:1142-8. https://doi.org/10.1016/j.jse.2014.12.017
21. Kerrigan AM, Reeves J, Langohr GDG, Johnson JA, Athwal GS. Reverse shoulder arthroplasty glenoid lateralization influences scapular spine strains. Shoulder Elbow 2021;13:610-9. https://doi.org/10.1177/1758573220935567
22. Knighton TW, Chalmers PN, Sulkar HJ, Aliaj K, Tashjian RZ, Henninger HB. Reverse total shoulder glenoid component inclination affects glenohumeral kinetics during abduction: a cadaveric study. J Shoulder Elbow Surg 2022;31:2647-56. https://doi.org/10.1016/j.jse.2022.06.016
23. Knighton TW, Chalmers PN, Sulkar HJ, Aliaj K, Tashjian RZ, Henninger HB. Anatomic total shoulder glenoid component inclination affects glenohumeral kinetics during abduction: a cadaveric study. J Shoulder Elbow Surg 2022;31:2023-33. https://doi.org/10.1016/j.jse.2022.03.028
24. Knowles NK, Ferreira LM, Athwal GS. Premorbid retroversion is significantly greater in type B2 glenoids. J Shoulder Elbow Surg 2016;25:1064-8. https://doi.org/10.1016/j.jse.2015.11.002
25. Knowles NK, Keener JD, Ferreira LM, Athwal GS. Quantification of the position, orientation, and surface area of bone loss in type B2 glenoids. J Shoulder Elbow Surg 2015;24:503-10. https://doi.org/10.1016/j.jse.2014.08.021
26. Kocsis G, Thyagarajan DS, Fairbairn KJ, Wallace WA. A new classification of glenoid bone loss to help plan the implantation of a glenoid component before revision arthroplasty of the shoulder. Bone Joint J 2016;98-B:374-80. https://doi.org/10.1302/0301-620X.98B3.36664
27. Kose O, Canbora MK, Koseoglu H, Kilicoglu G, Turan A, Yuksel Y, et al. Can we use the contralateral glenoid cavity as a reference for the measurement of glenoid cavity bone loss in anterior shoulder instability?. A comparative analysis of 3d ct measurements in healthy subjects. Int J Morphol 2018;36:1202-5. https://doi.org/10.4067/S0717-95022018000401202
28. Lévigne C, Boileau P, Favard L, Garaud P, Molé D, Sirveaux F, et al. Scapular notching in reverse shoulder arthroplasty. J Shoulder Elbow Surg 2008;17:925-35. https://doi.org/10.1016/j.jse.2008.02.010
29. Lewis GS, Armstrong AD. Glenoid spherical orientation and version. J Shoulder Elbow Surg 2011;20:3-11. https://doi.org/10.1016/j.jse.2010.05.012
30. Moineau G, Levigne C, Boileau P, Young A, Walch G. Three-dimensional measurement method of arthritic glenoid cavity morphology: feasibility and reproducibility. Orthop Traumatol Surg Res 2012;98(SUPPL 6):S139-45. https://doi.org/10.1016/j.otsr.2012.06.007
31. Neer CS, Craig EV, Fukuda H. Cuff-tear arthropathy. J Bone Joint Surg 1983;65:1232-44.
32. Neyton L, Gauci MO, Deransart P, Collotte P, Walch G, Athwal GS. Three-dimensional characterization of the anteverted glenoid (type D) in primary glenohumeral osteoarthritis. J Shoulder Elbow Surg 2019;28:1175-82. https://doi.org/10.1016/j.jse.2018.09.015
33. Nyffeler RW, Sheikh R, Atkinson TS, Jacob HAC, Favre P, Gerber C. Effects of glenoid component version on humeral head displacement and joint reaction forces: an experimental study. J Shoulder Elbow Surg 2006;15:625-9. https://doi.org/10.1016/j.jse.2005.09.016
34. Parada SA, Paynter JW, Paré DW, Amero JJ, Kyrkos JG, Broxton GA, et al. Use of the contralateral glenoid for calculation of glenoid bone loss: a cadaveric anthropometric study. Arthroscopy 2020;36:1517-22. https://doi.org/10.1016/j.arthro.2020.01.049
35. Plessers K, Vanden Berghe P, Van Dijck C, Wirix-Speetjens R, Debeer P, Jonkers I, et al. Virtual reconstruction of glenoid bone defects using a statistical shape model. J Shoulder Elbow Surg 2018;27:160-6. https://doi.org/10.1016/j.jse.2017.07.026
36. Plessers K, Verhaegen F, Van Dijck C, Wirix-Speetjens R, Debeer P, Jonkers I, et al. Automated quantification of glenoid bone defects using 3-dimensional measurements. J Shoulder Elbow Surg 2020;29:1050-8. https://doi.org/10.1016/j.jse.2019.10.007
37. Ricchetti ET, Hendel MD, Collins DN, Iannotti JP. Is premorbid glenoid anatomy altered in patients with glenohumeral osteoarthritis? Clin Orthop Relat Res 2013;471:2932-9. https://doi.org/10.1007/s11999-013-3069-5
38. Salhi A, Burdin V, Boutillon A, Brochard S, Mutsvangwa T, Borotikar B. Statistical shape modeling approach to predict missing scapular bone. Ann Biomed Eng 2020;48:367-79. https://doi.org/10.1007/s10439-019-02354-6
39. Scalise JJ, Bryan J, Polster J, Brems JJ, Iannotti JP. Quantitative analysis of glenoid bone loss in osteoarthritis using three-dimensional computed tomography scans. J Shoulder Elbow Surg 2008;17:328-35. https://doi.org/10.1016/j.jse.2007.07.013
40. Scalise JJ, Codsi MJ, Bryan J, Iannotti JP. The three-dimensional glenoid vault model can estimate normal glenoid version in osteoarthritis. J Shoulder Elbow Surg 2008;17:487-91. https://doi.org/10.1016/j.jse.2007.09.006
41. Shapiro TA, McGarry MH, Gupta R, Lee YS, Lee TQ. Biomechanical effects of glenoid retroversion in total shoulder arthroplasty. J Shoulder Elbow Surg 2007;16(3 SUPPL):S90-5. https://doi.org/10.1016/j.jse.2006.07.010

42. Sharif-Ahmadian A, Beagley A, Pearce C, Saliken D, Athwal GS, Giles J. Statistical shape and bone property models of clinical populations as the foundation for biomechanical surgical planning: application to shoulder arthroplasty. J Biomech Eng 2023;145:101004. https://doi.org/10.1115/1.4062709
43. Shi L, Griffith JF, Huang J, Wang D. Excellent side-to-side symmetry in glenoid size and shape. Skeletal Radiol 2013;42:1711-5. https://doi.org/10.1007/s00256-013-1728-y
44. Sirveaux F, Favard L, Oudet D, Huquet D, Walch G, Molé D. Grammont inverted total shoulder arthroplasty in the treatment of glenohumeral osteoarthritis with massive rupture of the cuff. Results of a multicentre study of 80 shoulders. J Bone Joint Surg Br 2004;86:388-95. https://doi.org/10.1302/0301-620X.86B3.14024
45. Soltanmohammadi P, Elwell J, Veeraraghavan V, Athwal GS, Willing R. Investigating the effects of demographics on shoulder morphology and density using statistical shape and density modeling. J Biomech Eng 2020;142:121005. https://doi.org/10.1115/1.4047664
46. Sugaya H. Techniques to evaluate glenoid bone loss. Curr Rev Musculoskelet Med 2014;7:1-5. https://doi.org/10.1007/s12178-013-9198-3
47. Verhaegen F, Meynen A, Debeer P, Scheys L. Determination of predisposing scapular anatomy with a statistical shape model—Part II: shoulder osteoarthritis. J Shoulder Elbow Surg 2021;30:e558-71. https://doi.org/10.1016/j.jse.2021.01.018
48. Verhaegen F, Meynen A, Matthews H, Claes P, Debeer P, Scheys L. Determination of pre-arthropathy scapular anatomy with a statistical shape model: part I—rotator cuff tear arthropathy. J Shoulder Elbow Surg 2021;30:1095-106. https://doi.org/10.1016/j.jse.2020.07.043
49. Verhaegen F, Meynen A, Pitocchi J, Debeer P, Scheys L. Quantitative statistical shape model-based analysis of humeral head migration, part 2: shoulder osteoarthritis. J Orthop Res 2022;41:21-31. https://doi.org/10.1002/jor.25335
50. Verhaegen F, Meynen A, Plessers K, Scheys L, Debeer P. Quantitative SSM-based analysis of humeral head migration in rotator cuff tear arthropathy patients. J Orthop Res 2022;40:1707-14. https://doi.org/10.1002/jor.25195
51. Verhaegen F, Plessers K, Verborgt O, Scheys L, Debeer P. Can the contralateral scapula be used as a reliable template to reconstruct the eroded scapula during shoulder arthroplasty? J Shoulder Elbow Surg 2018;27:1133-8. https://doi.org/10.1016/j.jse.2017.12.024
52. Williams GR, Wong KL, Pepe MD, Tan V, Silverberg D, Ramsey ML, et al. The effect of articular malposition after total shoulder arthroplasty on glenohumeral translations, range of motion, and subacromial impingement. J Shoulder Elbow Surg 2001;10:399-409.
53. Wong MT, Langohr GDG, Athwal GS, Johnson JA. Implant positioning in reverse shoulder arthroplasty has an impact on acromial stresses. J Shoulder Elbow Surg 2016;25:1889-95. https://doi.org/10.1016/j.jse.2016.04.011
54. Zeng W, Lewicki KA, Chen Z, Van Citters DW. The evaluation of reverse shoulder lateralization on deltoid forces and scapular fracture risk: a computational study. Med Nov Technol Devices 2021;11:100076. https://doi.org/10.1016/j.medntd.2021.100076